Solid Freeform Fabrication 2018: Proceedings of the 29th Annual International Solid Freeform Fabrication Symposium – An Additive Manufacturing Conference
Reviewed Paper

QUANTIFYING THE EFFECT OF EMBEDDED COMPONENT ORIENTATION ON FLEXURAL PROPERTIES IN ADDITIVELY MANUFACTURED STRUCTURES

Swapnil Sinha[1], and Nicholas A. Meisel[2]

[1]Mechanical and Nuclear Engineering Department, Penn State, University Park, PA 16802
[2]School of Engineering Design, Technology, and Professional Programs, Penn State, University Park, PA 16802

ABSTRACT

In-situ embedding with Additive Manufacturing (AM) enables a user to insert functional components in a part by pausing the print, inserting the component into a specially designed cavity, and then resuming the print. This introduces the capability to merge the reliable functionality of external parts into AM structures, allowing multifunctional products to be manufactured in a single build. Previous research has shown that process interruption introduces weaknesses at the paused layer, and the presence of an embedding cavity further reduces the maximum tensile strength of the part. The research presented in this paper expands this understanding by investigating the impact of the process and design considerations for embedding on the strength of the material extrusion parts. A cuboidal geometry is embedded with different orientations with a flush surface at the paused layer, and tested for maximum bending strength. The findings help to further design guidelines for embedding with material extrusion AM.

1. INTRODUCTION

The layer-by-layer nature of AM provides an opportunity to embed sensors, actuators, circuits, and other functional components within a part, during the manufacturing process [1], [2]. This allows integration of reliable functionality of these components with creatively designed structures. However, AM is a relatively nascent method of manufacturing that cannot use the established standard design guidelines created for centuries-old traditional manufacturing processes. To realize the opportunities that AM promises in design and manufacturing of multifunctional components, this work seeks to address this particular gap of information in DfAM - embedding. This capability recently has been recognized for its application to the design and production of optimized parts and sophisticated "smart" objects [3]–[6].

Polymer material extrusion systems for AM allow for components to be embedded without subjecting them to damaging temperatures and pressures. The variety of thermoplastics available for material extrusion help to enable its wide application in various industries and make it a suitable candidate for in-situ embedding research. However, the temperature dependence of the structural properties [7]–[9] of created parts pose a process inherent constraint on overall quality of the part. The embedding process requires a cavity to be designed in the part and a process interruption step to have the components inserted completely inside the printed part. The combined influences of the intentionally designed cavity and the required process interruption pose questions for enabling design for embedding with AM in such a way that is not significantly detrimental to a printed part's mechanical properties. To answer these questions, this research work explores the design considerations with respect to orientation of the embedded geometry for produced parts under bending loads.

2. LITERATURE REVIEW

2.1 Multifunctional Parts via AM, Applications of Embedding Process

The recent explosive growth of the Internet of Things [10] has spurred AM research on the validation of form with functionality, which primarily involves embedding functional components in parts [11]–[14]. Technologies such as near-field communication, real-time localization, and feedback from embedded sensors have enabled the transformation of everyday objects into "smart" objects [15], [16]. AM makes embedding these sensors feasible and cost-effective. Integrating current technologies with AM allows for the design and production of sophisticated products in an automated manner and, therefore, with a reduced product development cycle time [11], [17]. For example, Macdonald et al. [11] developed an SLA process to 3D print electronics, Meisel et al. [2] demonstrated procedures for creating actuated joints by embedding shape memory alloys with the material jetting process, and Hahnlen and co-authors developed activated composite materials by seamlessly embedding smart materials with Ultrasonic Additive Manufacturing [18].

Traditional fabrication of functional components like sensors and actuators that leverage technologies like nanomaterials and microelectromechanical systems (MEMS), requires tailored manufacturing processes like chemical etching [19] or high current plasma beams [20]. Where AM allows for direct deposition of materials for multifunctional components due to its control of material at any point of the geometry [20]–[23], multiple process integrations are required to make it possible, and these materials must also satisfy the AM process requirements. For example, material extrusion process requires melting of the materials and solidification on deposition for which the materials have to be heated to high temperatures. While use of AM systems are possible for such fabrications, the technology has to still go a long way to compete with the reliability offered by traditional manufacturing of such components [24]. In-situ embedding is therefore a more near-term solution for creating multifunctional products via AM.

Zawaski and co-authors deemed in-situ embedding of medicine into a soluble shell created with material extrusion as a more feasible approach than direct deposition, which could damage the active medicine [25]. Fabrication of complex biological structures via AM was demonstrated by in-situ embedding of soft hydrogels in printed support material [26]. Macdonald et al. [27] demonstrated fabrication of smart products by combining direct deposition of interconnects with embedded electronics. This technique has also enabled applications like structural health monitoring (SHM) systems for structures like bridges, buildings, aircraft, and mega machines in which catastrophic failures must be avoided [28]. These potential application areas for in-situ embedding via AM often require high safety and performance standards, as well as careful process and quality control. Therefore, quality investigations are required to ensure its acceptance [29].

2.2 Design for Embedding Considerations and their Impact on Material strength

Embedding any component with AM requires the cavity to be designed such that the component is successfully and completely inserted in the cavity, before resuming the print. Therefore, the embedding cavity design depends greatly on the orientation of the component to be embedded. Changing orientations of the component requires corresponding changes in the design of the cavity, and could require need for shape converter (the filler geometry to create flush surface before resuming the print) [2]. An earlier study was performed to investigate the effects of process interruption and embedding on the tensile strength of printed parts [30]. The introduced weakness at the paused layer, as well as further reduction of part strength due to the designed cavity for embed, raises concern over design considerations for embedding.

Inter-layer bond strength is a major factor when it comes to the mechanical properties of 3D printed parts [2], [7], in-situ embedding impact's a structure's mechanical properties due to the inherent requirement of process interruption [30]. However, a review of the available literature shows that published research in this area is still sparse. Outside of AM, a study on the mechanical properties of cast epoxy resin with and without embedded silicon substrates verified that the ultimate tensile strength dramatically reduced when embedding was performed [31]. Also, the points of failure for each specimen were located at the embedded section. Flexural strength was found to be dependent on location of substrate in the cross section. Furthermore, the shape, size, orientation, and placements of defects in homogeneous parts are considered culprits for initiation and propagation of failures due to bending loads [32].

Due to multiple print parameters that introduce many variables, material extrusion process changes the final mechanical properties of the part from the original mechanical properties of the material. Quantifying these properties are important for informed design decisions. Since embedding process introduces a weakness due to the cavity and process interruption, design decisions should be carefully made to get the best possible part quality [30]. This work aims to understand the impact of orientation of the embedded geometry on flexural strength of the part, since tensile strength was found to be impacted due to presence of the cavity [30]. Since flexural strength was shown to be impacted by the location of the embedded substrate in the cross section for a cast epoxy part [31], it is highly possible for AM parts to be impacted similarly. Therefore, this paper looks into cavity orientations and its impact on flexural strength, such that informed design decisions can be made to create quality products via in-situ embedding.

2.3 Context

As this review shows, embedding application has shown need for design in accordance to process and part strength requirements. This research will start to address this gap by investigating the impact of different orientations of a cuboid on flexural strength of the part. Section 3 elaborates on the employed methodology and experiments. Section 4 discusses the results, and presents with Finite Element Analysis (FEA) simulations of the experiments. Section 5 wraps the research with the summary, and future work that this research suggests.

3. EXPERIMENTAL APPROACH

In order to provide a general understanding of part strength and embedding cavity design relationships, geometries have to be carefully selected, such that these understandings can be applied as design guidelines for future geometry. Components like sensors, actuators, and batteries, that are envisioned to be embedded for multifunctional application with AM [24] have various shapes and sizes. However, all these components are mostly combinations of primitive shapes like cuboids, cylinders, spheres, wedges, cones, tetrahedrons, etc. Therefore, to initiate the creation of standard design guideline for embedding components with AM, a cuboidal geometry is targeted in this paper. The following sub sections discuss the investigated research questions, and the experimental methods employed.

3.1 Research Questions (RQ)

For embedding applications, the design of the cavity for embedding a component requires careful consideration of the process type and shape of the component. This research explores the embedding orientations for the most basic embeddable geometry with a flush surface. From here on these types of component geometries will be referred as flush geometries.

Multiple orientations are possible for flush geometries, each may impact the overall material properties of the part due to the inherent anisotropy. This exploratory work investigates this behavior of AM parts under flexural loading, with controlled embedding cavity designs for a cuboid. For this purpose, the impact of process interruption on flexural strength is first studied to predict its influence on embedded specimens. The following research questions will be answered through this study:

- **RQ1. To what extent does process interruption influence flexural strength of the AM produced part?** Process interruption was found to be detrimental for tensile strength of the part. Since embedding process requires process interruption, quantification of its impact on flexural strength is essential to predict its impact on embedded parts.
- **RQ2. To what extent does orientation of a cuboidal geometry, with a flush surface at the resumed layer, impact the flexural strength of the part?** Different orientations of a cuboidal geometry offer different cross section area, cavity depth, and wall thicknesses. Understanding these influences are essential for informed design decisions for multifunctional products with AM.

3.2 Experimental Setup

The embedding process requires process interruption after the cavity is printed, and it has been found to negatively impact the tensile strength. It is necessary to quantify the effects of process interruption on flexural strength to better understand the behavior of the structure with designed cavities and embeds, when subjected to a variety of loading conditions. For this purpose, specimens of dimension 24 mm x 12 mm x 96 mm were prepared with a MarkOne material extrusion 3D printer and manufactured with nylon material. To directly compare the flexural performance with the tensile performance obtained from the earlier research [30], the specimen design and manufacturing parameters were kept consistent with a layer height of 0.2 mm and 100% infill density. The specimens were printed upright with the length (96 mm) along the Z- axis of the build plate. This orientation allows for leveraging the material anisotropic effect to the research's benefit. The weaker strength across the layers, makes the overall part more sensitive to embedding process and its effects. Specimens were accordingly designed and produced with different treatments, namely the Control, Paused, Embedded, and Cavity specimens. The Control specimens were prepared with no interruptions or cavity, serving as the baseline for comparison. The Paused specimens were subjected to process interruption for > 5 minutes at the center layer. The Embedded specimens were prepared with the designed cavities to capture effects of orientation of the embedded cuboid. The specimens were paused once the cavity was printed, inserted with the embed at its respective orientation, and resumed after 5 minutes of process interruption. The Cavity specimens were produced with only the cavity, the print was interrupted once the cavity was printed and resumed after 5 minutes. The Cavity specimens allow to capture the effects of inserted component on flexural strength of the part, by their direct comparison with the Embedded specimens.

When given a 90° rotation in roll, pitch and yaw, a cuboid with different values for length, width, and height gives six different possible orientations. Each of its six symmetric orientations offer three different cross-sections and depths, which act as independent variables for the study (Figure 1.). Direct comparisons of maximum flexural strength values as the dependent variable can lead to determination of the impact of cross-section and cavity depth on material strength.

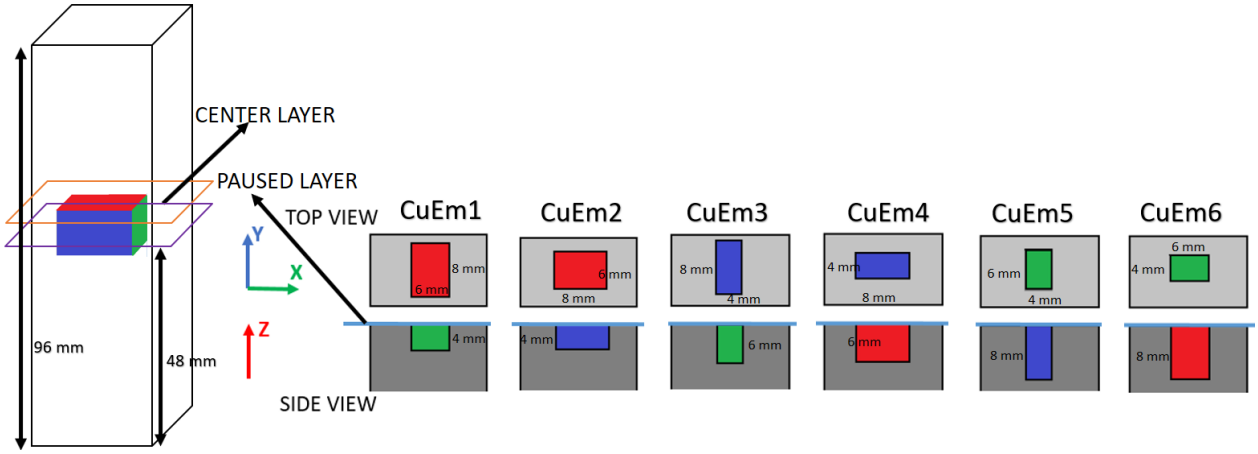

Figure 1. Shows the cuboidal embed with different length, breadth, and height.

To capture the effects of its different orientations, it was necessary to ensure that the cross section of the cavity varied consistently, and was physically feasible to embed by the user. The dimension for the cuboid embed was therefore selected as 4 mm x 6 mm x 8 mm, so as to fit in the cross section of the designed specimen (24 mm x 12 mm), in all of its six different orientations, and be successfully manufactured. The CuEm3 were produced with an empty cavity for the Cavity specimens. The cuboid embed was produced with the same system and parameters as the specimens. All the embedding cavities were located at the geometric center of the specimen.

4. RESULTS AND DISCUSSION

Three point bending tests were performed on the produced specimens with an MTS screw driven load frame and 15kN load cell. The span length was set as 44 mm, in order to load the same gage length as in the tensile test specimens in previous work [30]. A displacement rate of 0.5mm/min was set for the load, and six specimens for each group were tested until failure. Experimentally obtained data for maximum flexural load was statistically compared to identify significant differences answering each research question, and are elaborated in the following sub sections.

4.1 Effects of Process Interruption on Flexural Strength of the Specimen

After removal of two outlier data points, the maximum flexural load obtained for seven samples each for Control and Paused specimens were analyzed for differences with a Mann Whitney U Test. The analysis showed that paused specimens had significantly lower maximum flexural load than the control specimens ($p<0.025$), indicating the expected influences of process interruption [30] on flexural strength of the part. The paused specimens failed repeatedly at the paused layer, unlike the control specimens. The maximum flexural strength, was obtained from the experimental load values from the equation:

$$\sigma = -\frac{My}{I} \tag{I}$$

Where M is the moment at the cross section, y is the distance of the surface from neutral axis, and I is the moment of inertia of the cross section being investigated. Interestingly, for both the control and paused specimens, the maximum flexural strength was found to be approximately

twice of the tensile strength of the similarly produced parts in previous research (Figure 2.), which is expected to be the same for ideal isotropic materials. Similar differences between the flexural and tensile strength values were found in the parametric study by Sood et. al [33] for specimens produced with acrylonitrile butadiene styrene (ABS) material on material extrusion systems.

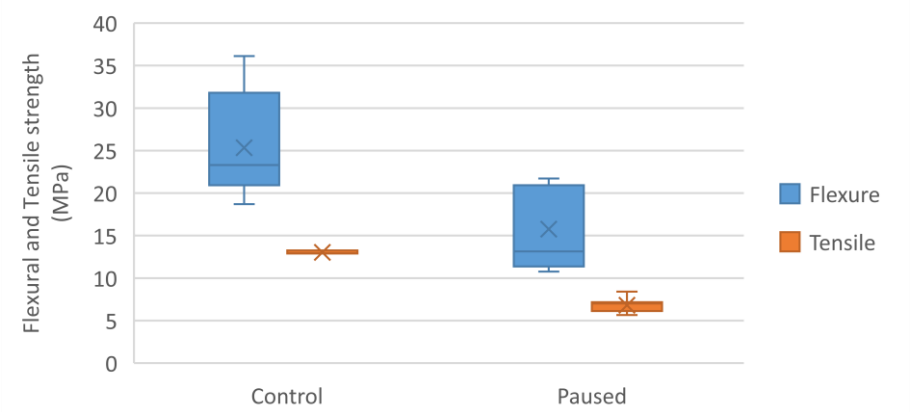

Figure 2. Shows distribution of maximum strength values in case of 3 point bending and tensile testing [30].

During 3 point bending tests, the specimen undergoes varying stresses at its cross section. The outermost surface of the cross section at the center layer undergoes the maximum tensile stress (obtained from equation (I)). The crack at failure propagates from the outermost layer, indicating that the loads at failure are determined by the strength of the outermost surface. The higher values for the flexural strength in case of both the Control (28.68±10.53 MPa) and the Paused (16.66±4.67 MPa) specimens, than their tensile strength values (Control=13.027±0.16 MPa, and Paused =7.06±0.92 MPa), can be explained by the cross sectional view of the specimens. Where the deposited roads for the wall has no air gap between them, the deposited roads in the infill show air gaps throughout, as shown in Figure 3. (b), where a deposited cross section was examined by shading it with permanent black marker. The shading highlights the top layer in black, and the white material from the other layers are visible due to air gaps. Such air gaps have been characterized detrimental for the part strength [33]–[35], which could offer an explanation to this improved flexural strength, where only the dense wall of the specimens are tested for failure.

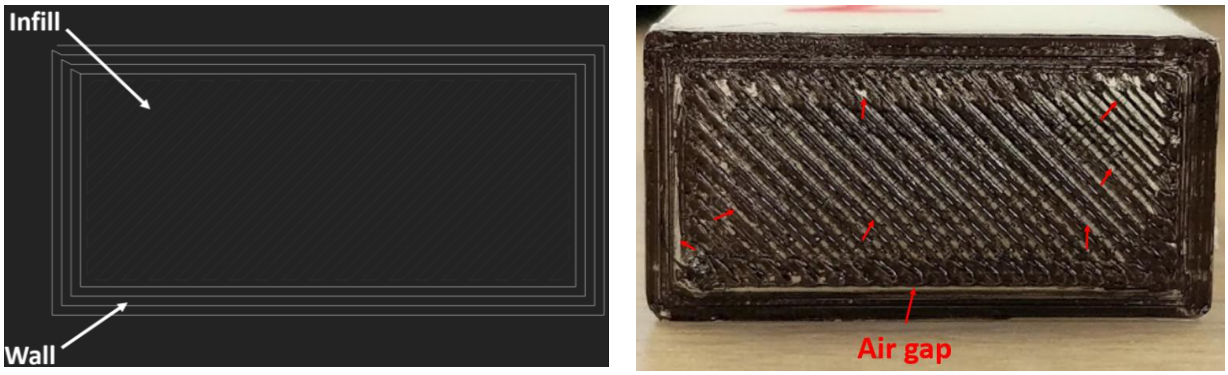

(a) (b)

Figure 3. Shows the cross sectional view of the specimen's (a) tool path and (b) cross section.

Further analysis of the cross section at failure showed differences between the Control and the Paused specimens. Where the deposited layers for the Control specimens were able to provide a better weld strength between the layers, evident by the delamination in multiple layers, the Paused specimens showed delamination of only the paused layer (Figure 4). The temperature history of the deposited layer has been found effective in predicting strength of the parts for both ABS and polycarbonate materials, common in material extrusion systems [7]. This provides an explanation to the weaknesses due to the cooled layer because of process interruption.

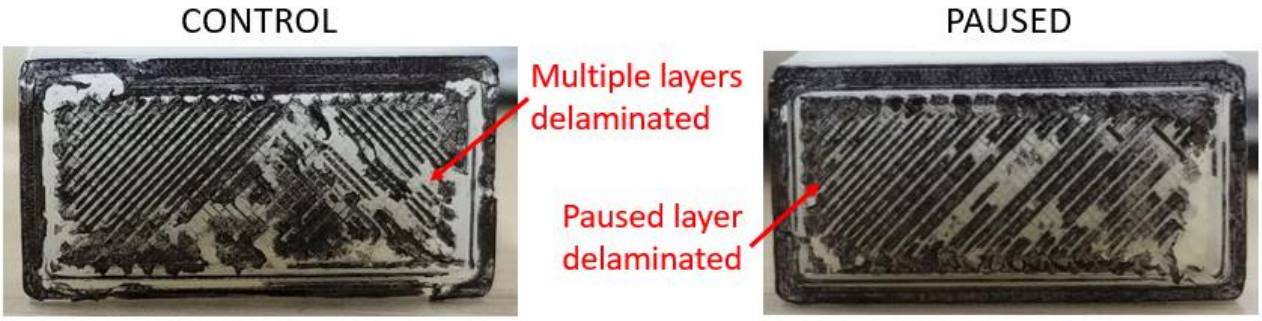

Figure 4. Cross sections of the delaminated layer of the failed specimens showing varying degrees of failure for Control and Paused specimens.

As discussed in the literature review, applications of embedding with AM show embedding with variety of materials of complex geometries. The designed cavities for such geometries will require advanced analysis of stress distribution, in order to evaluate design alternatives. In case of traditionally manufactured structures and materials, computational tools like FEA offer practical solutions to designers in case of complex designs. However, due to multiple variable parameters and complexities involved in an AM manufactured part, FEA modelling of the specimens to the details demands high computational requirements. Therefore, the use of a simple isotropic assumption for the material properties was evaluated for the designed groups. COMSOL Multiphysics – Solid Mechanics with Static study was used to simulate the three point bend test for the specimen designed for Control and Paused group, using the experimentally obtained maximum flexural load. For simulation, only half of the specimen's span length (22 mm) was modelled with isotropic properties of built in Nylon material, where the density (1.1 kg/m^3) and young's modulus (1130 MPa) were provided based on prior work with tensile properties [30]. A symmetry condition was applied at the face, i.e. the centermost plane of the specimen, which adds a boundary condition representing symmetry in geometry and loads about that plane. The model was given an edge loading condition of half the value of experimentally obtained flexural load, to account for the symmetry on that plane. Additionally, the edge diametrically opposite to the loaded edge was given a zero displacement condition vertically, and sideways.

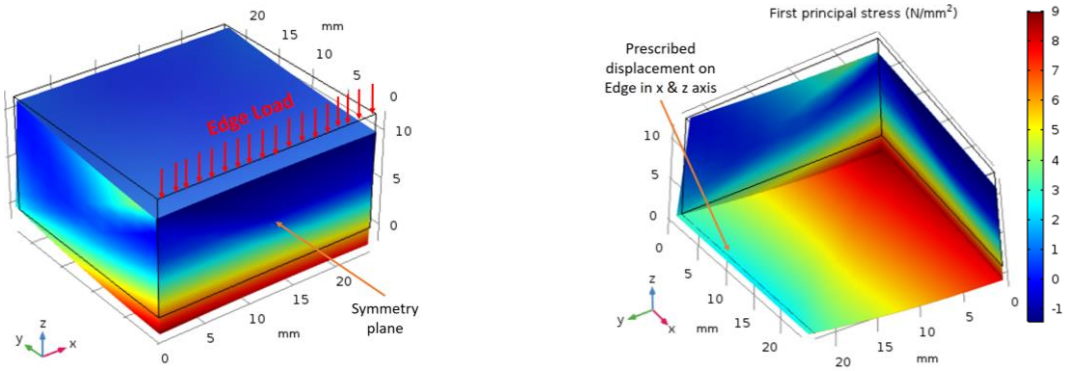

(a) (b)

Figure 5. FEA simulation of three point bend test on half of the specimen, with symmetry condition where (a) and (b) show different views of the same model.

Mesh convergence studies show convergence at the finer mesh elements and the error convergence plots show reduced errors to 0.02% after 20 iterations. The obtained stress output from FEA at the outermost surface of the center layer was compared with theoretically obtained stress from eq (I), for experimentally obtained maximum flexural load values. The simulation was successfully validated with an error within 5% from the calculated stress (Figure 6.). This agreement in the FEA and theoretically obtained stress values, serves as a calibration for FEA of AM parts with isotropic material assumption. This means that similar methodology can be employed for complex designs, where theoretical estimations are difficult. FEA suggests that maximum tensile stresses occur at the outermost surface of the cross section which is loaded in the specimen. Experimentally, the location of failure for control specimens were within ±2mm from the center, propagating through multiple layers (as shown in Figure 4.). For paused specimens, there was a clear delamination at the paused layer, which was the loaded cross section.

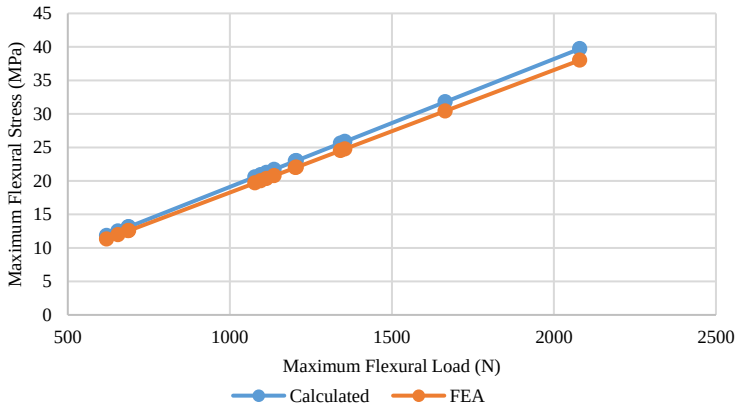

Figure 6. Validation of the FEA simulation for three point bending for Control and Paused specimens.

4.2 Effects of Orientation of a Cuboid on Flexural Strength

In order to reduce the redundancy in experimentation, only four out of the six groups were produced with six repetitions; CuEm1, CuEm3, CuEm4, and CuEm5. These four orientations explore three different cavity cross sectional areas, wall thicknesses, and cavity depths designed

for embedding (See Table 1.). Even though the theory suggests that specimens should fail at the location of maximum moment [36] which is at the centermost layer, the three-point bend tests showed a consistent failure location at the paused layer for all the embedded specimens. This signifies the influence of weakness at the paused layer. Using the knowledge that the process interruption makes the paused layer the weakest layer in these embedded specimens, theoretical predictions of the load at failure were done for the designed specimens at their weakest layer. The average of the experimental maximum flexural strength values σ_{paused}, obtained for the paused specimens (15.51±4.36 MPa) was used as the predictor for maximum flexural load (F) that causes failure for each of the designed embedded specimen. Using equation (I),

$$\sigma_{paused} = -\frac{(\frac{F}{2}\times(\frac{\frac{L}{2}+\frac{h}{2}}{2})-F\times\frac{h}{2})\frac{t}{2}}{\frac{wt^3}{12}-\frac{db^3}{12}} = -\frac{F\times(\frac{L-h}{4})\frac{t}{2}}{\frac{wt^3}{12}-\frac{db^3}{12}} = -\frac{F}{c} \quad \text{(II)}$$

$$\frac{1}{c} = \frac{(\frac{L-h}{4})\frac{t}{2}}{\frac{wt^3}{12}-\frac{db^3}{12}} \quad \text{(III)}$$

In these equations, w × t is the cross section of the specimen, d × b × h are the dimensions of the embedding cavity, and L is the span length for three point bend test. The area moment of inertia I for the embedded specimens at their paused layer was calculated by assuming the presence of the designed cavity at its geometric center (See Figure 1.). This estimated theoretical load at failure for each group was compared with the experimentally obtained values, the error for which varied from 2% to 50%, indicating the variation in the quality of the produced specimens (Table 1.).

Table 1. Comparing theoretical and experimental maximum flexural load, as estimated through maximum flexural strength for the paused specimens.

Groups	c/s Area (mm^2)	Wall thickness (mm)	Depth (mm)	Theoretical F from eq. (II) (N)	Experimental Load (N)	Error %	c eq. (III)
CuEm4	24	4	8	982.81	490.84±185.16	50%	63.41
CuEm3		3		971.33	1031.84±185.16	6%	62.66
CuEm5	32	2	6	893.38	631.84±337.16	29%	57.64
CuEm1	48		4	826.67	570.84±570.16	31%	53.33

The constant c is the multiplication factor that accounts for the location of failure according to the cavity's depth and area moment of inertia for that layer, which changes with each orientation. Statistical analysis of the obtained experimental values showed that all the embedded specimens show a significant difference in maximum flexural load values, when compared with the Control specimens ($p<0.005$). When compared with the paused specimens, the differences in the load values were not statistically significant for the samples from groups CuEm3 ($p>0.628$), CuEm5 ($p>0.53$), and CuEm1 ($p>0.222$). Even though the CuEm4 specimens were found to show a collectively lower flexural load values than the paused specimens, this difference was not found to be statistically significant ($p>0.0727$).

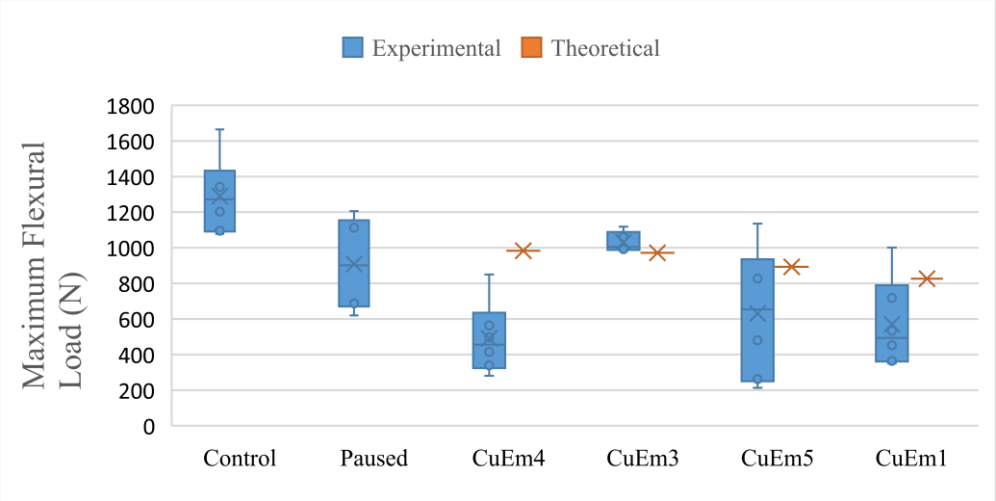

Figure 7. Experimentally obtained Maximum flexural load for each groups, compared with theoretically estimated load at failure as per the paused layer, for the embedded specimens.

The theoretically obtained flexural load at failure (Table 1.) show a trend between the groups, indicating that theoretically, different orientations of the cuboidal embed should have different values for maximum flexural load. The experimentally obtained load values for CuEm3, CuEm5, and CuEm1 show a similar trend, however, the statistical analysis do not signify the differences between these groups. The CuEm3 specimens showed a significantly higher flexural load values from the CuEm4 specimens ($p<0.019$), which could be attributed to the low quality samples for the group CuEm4. But all the other embedded group differences were statistically insignificant.

The observed reduced flexural load values for the CuEm4 specimens were further investigated, due to its high offset from the predicted value. Qualitative analysis of the failed layer revealed that three of the four samples prepared for this group showed low quality resumed layer; the deposited resumed layer showed thinner roads and as a result, wider air gap (Figure 8.). The one good sample with none of these defects, demonstrated a higher strength value than all the other three specimens. The defects are indicative of a clogged nozzle or insufficiently heated material, commonly caused in printers due to wearing after multiple uses. The added weakness at the paused layer along with the defects cause a detrimental effect on the embedded part's strength, which signifies the importance of the quality of the paused interface.

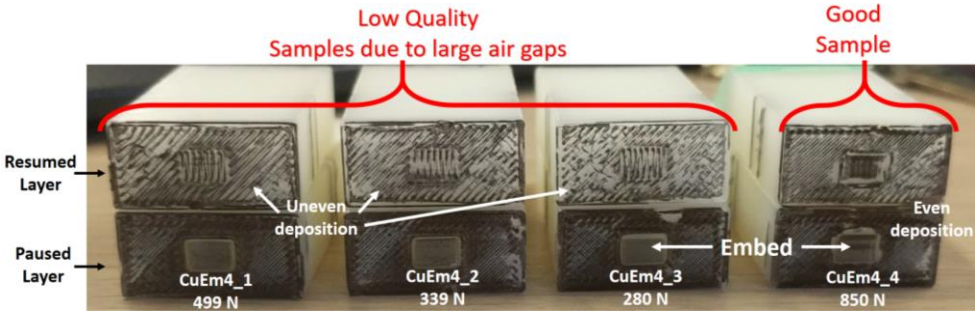

Figure 8. Cross sectional view of the failed specimens for each sample of CuEm4, with corresponding maximum flexural load.

Qualitative analysis of the failed specimens for all the groups indicate that the air gaps were consistently present for the specimens with lower maximum flexural load values. As shown in Figure 9. (a), the CuEm5 specimens that show lower flexural load values also demonstrate an unevenly resumed layer. As a result, this group also demonstrates a larger standard deviation. The group CuEm3 (Figure 9. (b)) with six repetitions, show no defects in their resumed layer, and as a result, a smaller standard deviation. The experimental flexural load value for this group showed only a 6% error from the predicted value.

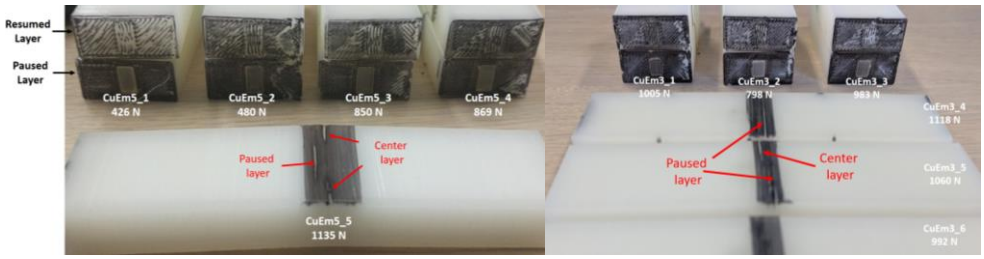

(a) (b)

Figure 9. Failed specimens for the embedded group (a) CuEm5 and (b) CuEm3

These analyses show the prevalence of defects on part quality in terms of material strength. Even though the statistical analysis show no significant differences between the different embedded groups, the observed trend indicates an effect of orientation on flexural strength of the parts. In these specimens, different orientations led to different locations of the paused layer, as well as different area moment of inertia due to the cavity, which is represented in the constant c (Table 1.). In general, it can be concluded that the placement of the cavity is a crucial factor, as it determines the location of the weakness due to process interruption. Also, the cavity should be such designed that it offers the highest area moment of inertia at the weakest layer for maximum flexural performance.

For load sensitive components to be embedded in the cavity, understanding how this integration of foreign components could influence the flexural strength is important. Therefore, three specimens of the same design as group CuEm3 were produced with just an empty cavity, but with a process interruption for 5 minutes after the cavity was printed. This group (Em3) was tested for flexural strength and compared with the flexural load values for the group CuEm3. The analysis shows no significance in the differences between the groups ($p>0.095$), which could be due to limitation in number of specimens. However, the observations suggest that the embedded component could potentially play a role in improving the flexural strength of the parts (Figure 10). The presence of the cavity causes stress concentrations around it, but the embedded material could have assisted in load dissipation. This indicates that the embedded material goes through stress while the part is being loaded, and due to the location of the weakest layer on top of its cavity, the embedded material plays a crucial part in determining the strength of the overall part.

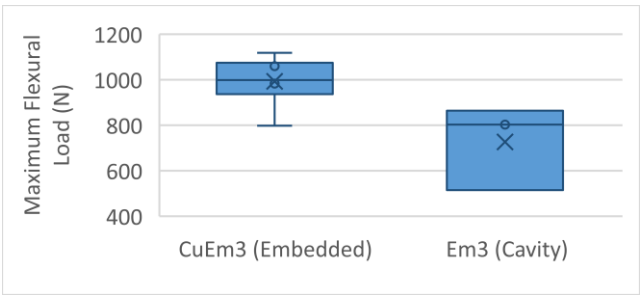

Figure 10. Comparing the maximum flexural load for embedded and cavity specimens.

The previous subsection concluded a successful simulation of the three point bend test for continuous specimens (Control and Paused). To evaluate applicability of FEA tool with isotropic material assumption for embedded specimens, a similar study was run for the Embedded and Cavity specimens. For added complexity in the model with the designed cavity and presence of an embedded component, the point of interest is the outermost surface of the paused layer (the known weakest layer). The simulation included a cavity design, and an assembled embedded block of the same size as the cavity. Since the experimentally prepared specimens were embedded at the geometric center, half of the cavity and corresponding embed was placed at the surface of the center plane. A contact boundary condition was applied for the surfaces of embed in contact with the part. Symmetry was again enabled for all the faces at the center plane (both the embed and the part). FEA was performed on each of the embedded specimen design using the experimental load values to identify the stress at the point of interest. A cavity specimen (Em3) with no embed and only cavity was also analyzed. The obtained values for each orientation were compared with that of theoretically obtained stress from equation (II).

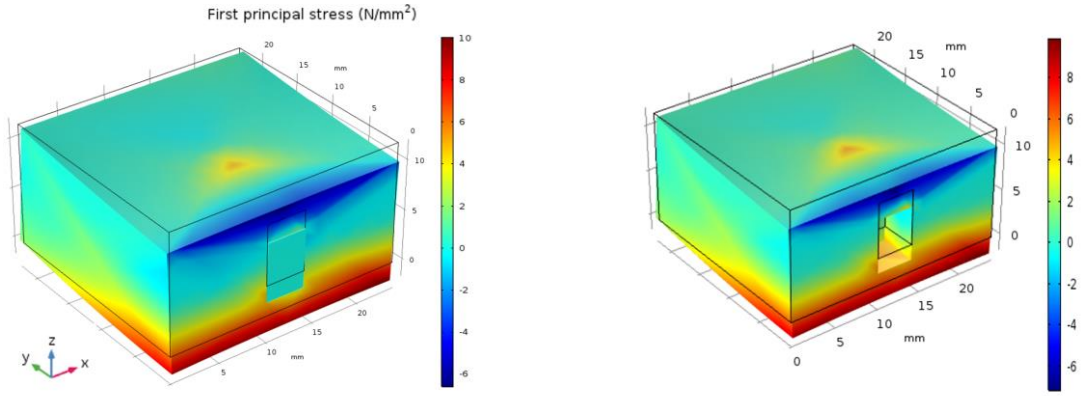

(a) (b)

Figure 11. FEA simulation of 3 point bending on (a) Embedded CuEm3, and (b) Cavity Em3 specimens.

The error in estimation for each of the embedded group varied from 1% to 7%, however the Em3 group showed a 0% error. This could be because of approximation of the embedded component as a cavity (in equation (II)), for theoretically obtained stress values. On the other hand, FEA simulates the presence of the embedded component through its boundary condition of contact between the cavity and the embedded component. The low error values indicate that the FEA simulation for a simple isotropic material condition is a valid predictor for stresses, when

investigating design considerations for embedding with AM. This means for complex cavity designs, where theoretical predictions are difficult, FEA can serve as a convenient tool for design evaluation. However, the FEA of the layer of process interruption has to be additionally performed for a realistic evaluation of AM produced parts.

5. KEY FINDINGS AND FUTURE WORK

This research investigated the flexural strength of the AM parts to quantify effects of embedding a cuboid with different orientations, as well as validated the FEA modelling for predicting the strength for embedded specimen. The cuboid serves as the most basic primitive geometry that provides a flush surface, and allows the study without the need for shape converters. Three point bend tests on specimens created to study effects of orientation of an embedded cuboid concludes the following:

- The maximum flexural strength is higher than the maximum tensile strength for AM parts printed upright, with and without the process interruption, as has been reported in earlier research [33], [37].
- Process interruption reduced the maximum flexural strength of the part to 58% by introducing weakness at the paused layer.
- FEA simulations with isotropic material assumption is valid for specimens with embedded components (error < 7%), due to known location of the weakest layer.

It can be concluded that knowledge of weakness at the paused layer can be greatly leveraged as a guide for comparing different designs for embedding with AM. The flexural strength of the paused layer were used to predict the maximum flexural load for the embedded specimens. Qualitative analysis show that experimental maximum flexural load values for embedded specimens show a similar trend as theoretically predicted values. However, the data points were limited in quantity to conclude this statistically. The presence of embed in the cavity also demonstrated slightly higher strength values than the specimens with just the cavity, hinting towards stress concentration dissipation around the cavity due to presence of the embedded material.

The findings provide a wide scope of future work, especially for inter layer bond strength at the paused layer. While re-heating has shown to improve the tensile strength [30], it could be damaging for the embedded component. Re-enforcement and adhesives provide another avenue to address the weakness due to process interruption. Additionally, more geometries for embedded components can be explored to better understand the influence of the cavity designs on material properties. As discussed, the non-flush geometries require shape converters, which can be designed in multiple ways, and thus would also benefit from further investigation. The validated FEA simulation serves as a calibration, to employ computational analysis of AM produced parts for embedding, with the known weakness of the paused layer.

6. REFERENCES

[1] V. Kumar, S. Rajagopalan, M. R. Cutkosky, and D. Dutta, “Representation and Processing of Heterogeneous Objects for Solid Freeform Fabrication,” *Geom. Model. Work.*, pp. 1–21, 1998.

[2] N. A. Meisel, A. M. Elliott, and C. B. Williams, “A procedure for creating actuated joints via embedding shape memory alloys in PolyJet 3D printing,” *J. Intell. Mater. Syst. Struct.*, vol. 26, no. 12, pp. 1498–1512, 2015.

[3] M. Leu, H. Xiao, and J. Dong, “Additive Manufacturing of Smart Parts with Embedded

Sensors for In-Situ Monitoring in Advanced Energy Systems Investigators : Program Manager :," 2015.
[4] S. Geller and M. Gude, "Process-Integrated Manufacturing and Embedding of Novel Piezoelectric Sensor Modules into Glass Fibre-Reinforced Polyurethane Composite Structures," *Mater. Sci. Forum*, vol. 825–826, pp. 563–570, Jul. 2015.
[5] R. R. J. Maier *et al.*, "Embedded fiber optic sensors within additive layer manufactured components," *IEEE Sens. J.*, vol. 13, no. 3, pp. 969–979, 2013.
[6] K. D. D. Willis, E. Brockmeyer, S. E. Hudson, and I. Poupyrev, "Printed Optics : 3D Printing of Embedded Optical Elements for Interactive Devices," *UIST '12*, pp. 589–598, 2012.
[7] J. Bartolai, T. W. Simpson, and R. Xie, "Predicting strength of additively manufactured thermoplastic polymer parts produced using material extrusion," *Rapid Prototyp. J.*, vol. 24, no. 2, pp. 321–332, 2018.
[8] C. Ajinjeru, V. Kishore, P. Liu, A. A. Hassen, and J. Lindahl, "Rheological evaluation of high temperature polymers to identify successful extrusion parameters," pp. 485–494, 2017.
[9] A. K. Ravi, A. Deshpande, and K. H. Hsu, "An in-process laser localized pre-deposition heating approach to inter-layer bond strengthening in extrusion based polymer additive manufacturing," *J. Manuf. Process.*, vol. 24, pp. 179–185, 2016.
[10] B. Sterling, *Shaping Things*, vol. 39, no. 5. London, England: MEDIAWORK, The MIT Press, 2005.
[11] E. MacDonald *et al.*, "3D printing for the rapid prototyping of structural electronics," *IEEE Access*, vol. 2, pp. 234–242, 2014.
[12] E. Aguilera *et al.*, "3D Printing of Electro Mechanical Systems," in *Proceedings of the 24th Solid Freeform Fabrication Symposium (SFF)*, 2013, pp. 950–961.
[13] K. B. Perez and C. B. Williams, "Combining Additive Manufacturing and Direct Write for Integrated Electronics – A Review," in *International Solid Freeform Fabrication Symposium Proceedings*, 2013, pp. 962–979.
[14] W. Gao, Y. Zhang, D. C. Nazzetta, K. Ramani, R. J. Cipra, and W. Lafayette, "RevoMaker : Enabling Multi-directional and Functionally-embedded 3D Printing using a Rotational Cuboidal Platform," in *Proceedings of the 28th Annual ACM Symposium on User Interface Software & Technology - UIST '15*, 2015, pp. 437–446.
[15] G. Kortuem, F. Kawsar, D. Fitton, and V. Sundramoorthy, "Smart objects as building blocks for the Internet of things," *Internet Comput. IEEE*, vol. 14, no. 1, pp. 44–51, 2010.
[16] A. C. Huebler *et al.*, "Ring oscillator fabricated completely by means of mass-printing technologies," *Org. Electron. physics, Mater. Appl.*, vol. 8, no. 5, pp. 480–486, 2007.
[17] D. Espalin, D. W. Muse, E. MacDonald, and R. B. Wicker, "3D Printing multifunctionality: Structures with electronics," *Int. J. Adv. Manuf. Technol.*, vol. 72, no. 5–8, pp. 963–978, 2014.
[18] R. Hahnlen and M. J. Dapino, "<title>Active metal-matrix composites with embedded smart materials by ultrasonic additive manufacturing</title>," *Proc. SPIE - Int. Soc. Opt. Eng.*, vol. 7645, p. 76450O–76450O–12, 2010.
[19] H. Xu, H. Zhang, Z. Deng, H. San, and Y. Yu, "Fabrication of Silicon Piezoresistive Pressure Sensor Using a reliable wet etching process," vol. 1, no. c, pp. 2–5.
[20] K. Watanabe *et al.*, "Plasma Ion-Beam 3D Printing : a Novel Method for Rapid Fabrication of Customized Mems Sensors," no. January, pp. 3–6, 2018.

[21] N. Hopkinson, P. Dickens, and N. Hopkinson, “Rapid prototyping for direct manufacture,” 2012.
[22] J. A. Lewis and G. M. Gratson, “Direct writing in three dimensions,” *Mater. Today*, vol. 7, no. 7, pp. 32–39, 2004.
[23] M. C. Frank *et al.*, “Direct Additive Subtractive Hybrid Manufacturing (DASH) Œ An Out of Envelope Method,” pp. 1853–1861, 2017.
[24] E. MacDonald and R. Wicker, “Multiprocess 3D printing for increasing component functionality.”
[25] C. Zawaski *et al.*, “Embedding of Liquids into Water Soluble Materials via Additive Manufacturing for Timed Release,” pp. 2047–2059, 2017.
[26] T. J. Hinton *et al.*, “Three-dimensional printing of complex biological structures by freeform reversible embedding of suspended hydr(1) Hinton, T. J.; Jallerat, Q.; Palchesko, R. N.; Park, J. H.; Grodzicki, M. S.; Shue, H.-J.; Ramadan, M. H.; Hudson, A. R.; Feinberg, A. W. Thr,” *Sci. Adv.*, vol. 1, no. 9, pp. e1500758–e1500758, 2015.
[27] E. Macdonald *et al.*, “3D Printing for the Rapid Prototyping of Structural Electronics,” vol. 2, 2014.
[28] J. Ihn and F. Chang, *Structural Health Monitoring*. 2008.
[29] I. Campbell, D. Bourell, and I. Gibson, “Additive manufacturing: rapid prototyping comes of age,” *Rapid Prototyp. J.*, vol. 18, no. 4, pp. 255–258, 2012.
[30] S. Sinha and N. A. Meisel, “Influence of process interruption on mechanical properties of material extrusion parts,” *Rapid Prototyp. J.*, p. RPJ-05-2017-0091, 2018.
[31] G. Dumstorff and W. Lang, “Failure of Silicon Substrates Embedded in Epoxy Resin,” *Procedia Technol.*, vol. 15, no. 0, pp. 216–220, 2014.
[32] Y. Murakami, “Material defects as the basis of fatigue design,” *Int. J. Fatigue*, vol. 41, pp. 2–10, 2012.
[33] A. K. Sood, R. K. Ohdar, and S. S. Mahapatra, “Parametric appraisal of mechanical property of fused deposition modelling processed parts,” *Mater. Des.*, vol. 31, no. 1, pp. 287–295, 2010.
[34] N. Holt, A. Vanhorn, M. Montazeri, and W. Zhou, “Microheater Array Powder Sintering : A Novel Additive Manufacturing Process,” pp. 1289–1313, 2017.
[35] S.-H. Ahn, M. Montero, D. Odell, S. Roundy, and P. K. Wright, “Anisotropic material properties of fused deposition modeling ABS,” *Rapid Prototyp. J.*, vol. 8, no. 4, pp. 248–257, 2002.
[36] A. C. Ugural and S. K. Fenster, *Advanced Mechanics of Materials and Applied Elasticity*. Pearson Education, 2011.
[37] J. S. F. S. U. FRASCATI, “EFFECTS OF POSITION, ORIENTATION, AND INFILTRATING MATERIAL ON THREE DIMENSIONAL PRINTING MODELS,” University of Central Florida Orlando, Florida, 2007.